Structures 68 (2024) 107227

Contents lists available at ScienceDirect

Structures

journal homepage: www.elsevier.com/locate/structures

Deformation mitigation and twisting moment control in space frames

Ahmed Manguri [a,b,*], Najmadeen Saeed [b,c], Robert Jankowski [a]

[a] Faculty of Civil and Environmental Engineering, Gdansk University of Technology, Gdansk, Poland
[b] Civil Engineering Department, University of Raparin, Rania, Iraq
[c] Civil Engineering Department, Tishk International University, Erbil, Iraq

ARTICLE INFO

Keywords:
Twisting moment
Shape control
Space frame
Optimization
Actuator

ABSTRACT

Over the last five decades, space frames have centered on the modernization of touristic zones in view of architectural attractions. Although attempts to control joint movement and minimize axial force and bending moment in such structures were made sufficiently, twisting moments in space frames have been underestimated so far. In space frames, external load or restoring the misshapen shape may cause twisting in members. We herein developed a robust computational algorithm to reduce the induced torsional moment through shape restoration within a desired limit by changing the length of active bars that are placed in space frames. Applying optimization algorithms like interior-point and Sequential quadratic programming (SQP), a direct correlation was pursued between bar length alteration and twisting in structural members. A numerical model of a single-layer space frame resembling an egg captures the twisting moment in all members, achieving a specified limit. The overall length change of the active members using an iterative process based on a heuristic that considers a threshold on the minimum length change of the active members.

1. Introduction

In the last five decades, constructing large space frames has become a feature of modern urban landscapes, seamlessly blending architectural finesse with artistic expression [1]. These structures, revered in architecture and structural engineering circles, revolutionize the approach to spanning vast areas. Space frames, characterized by their lightweight yet robust design, efficiently distribute loads across their framework, obviating the need for numerous internal supports [2]. Widely deployed in airports, exhibition halls, and sports arenas [3], space frames epitomize adaptability and versatility, enabling the realization of architectural designs. However, ensuring the safety of individual elements from the forces they endure presents a challenge in space frame engineering. Often, structures experience shape deformation under the action of external loadings. Researchers have been developing methodologies to overcome safety and serviceability problems by reducing the displacement response through the length change of active members.

Structural shape adjustment has been studied by a few researchers before the 90th, among them Weeks [4] and Haftka and Adelman [5]. Kwan and Pellegrino [6] reported the relationship between bar length change and axial force in members of space trusses; their study was based on the force method (FM) based on the Singular Value Decomposition of the equilibrium matrix (SVD-FM). In a study, Reksowardojo and Senatore [7] demonstrated the equivalence between the intuitive Integrated Force Method (IFM) and the computationally efficient Singular Value Decomposition Force Method (SVD-FM). Recently, Wang and Senatore [8] introduced a new method named the Extended Integrated Force Method (EIFM) to model the response of prestress-stable structures extending the IFM to kinematically indeterminate systems. Saeed and Kwan [9] proposed a study to control nodal displacements and axial forces simultaneously in pin-jointed assemblies. The study was developed to assign a domain for displacements of nodes in cables [10]. Shape control of a loaded cable structure was experimentally applied on a 3D cable net [11]. Regarding studies on shape control in space frames, an attempt has been made to reshape a single-layer egg-shaped dome space frame [12]. While research on adaptive structures has focused on truss systems, few studies have been conducted on adaptive tensioning systems for concrete slabs [13] and high-speed railway bridges [14] for efficient load management and significant material reduction. However, formulating the relationship of actuator length change to shape and internal forces previously studied in relation to adaptive structures [7,9], these studies were not interested in the effect of structural member length change on the twisting moment in space frames.

* Corresponding author at: Faculty of Civil and Environmental Engineering, Gdansk University of Technology, Gdansk, Poland.
E-mail address: ahmed.manguri@pg.edu.pl (A. Manguri).

https://doi.org/10.1016/j.istruc.2024.107227
Received 31 January 2024; Received in revised form 26 July 2024; Accepted 3 September 2024
Available online 6 September 2024

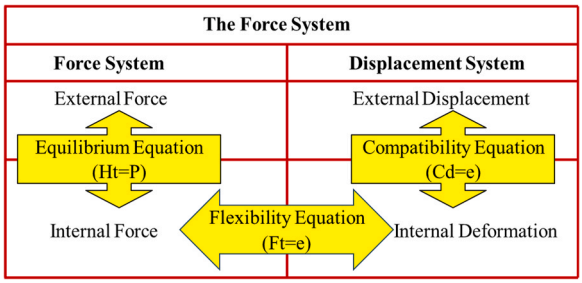

Fig. 1. The diagram of the force method system.

When it comes to structural optimization in adaptive structures, bar size optimization can be applied to cable and truss structures using actuators [15]. Recently, Senatore and Wang [16], formulated a new integrated structure-control All-In-One (AIO) method for topology optimization of adaptive structures. This method obtains global optima of the total system mass (structure + actuators) through simultaneous optimization of the structural topology, actuator placement, and control commands.

Different types of space frames and their analysis methodology were studied by Lan [17]. In addition, the analysis and design of space frames were presented by Ramaswamy *et al.* [18]. Furthermore, Galishnikova *et al.* [19] conducted a comprehensive study for finite element analysis applied to space frames, encompassing configurations with and without torsional restraints. The methodology entails delineating the orientation and approach for conducting first-order analyses on space frame elements. Generally, the twisting moment in structures involves the rotation of an element due to external loads, impacting stability and stress distribution within the structure [20,21]. Manguri *et al.* [22] reported mitigating bending moment in space frames by adding extra members in optimal locations.

When it comes to mitigation of twisting moments in frame structures, attention has been paid to the induced torsion caused by dynamic loadings. For instance, a study reported that a significant twisting moment developed during earthquakes in columns [23]. Likewise, another study reported the twisting moment in symmetric buildings derived from the soil-structure interaction [24]. Anagnostopoulos *et al.* [25] presented a detailed review of the effects of earthquake torsion on buildings. Several devices, such as triple-friction pendulum systems [26], multiple magnetorheological dampers [27], and multiple-tuned liquid dampers, have been investigated [28,29] to mitigate torsion-induced damages during earthquakes. However, dynamic loading is not the only source of torsion. Other sources exist, such as eccentric static loadings [30] and structural irregularity [31].

External loads and shape control can cause significant changes in twisting moments in space frames. So far, less attention has been paid to the influence of bar length change on the twisting moments. This study addresses the mitigation of deformation and twisting moments caused by external loads in space frames through shape restoration. The method developed and examined herein seeks to simultaneously control twisting moment and shape deformation in a single-layer egg-shaped space frame while minimizing the actuator length changes and computation time using the force method. The algorithm iteratively approaches minimum actuator length changes considering the constraints. It also attempts to iteratively eliminate ineffective actuators so as to reduce the number of implemented actuators.

2. Methodology

2.1. Method formulation

The proposed technique is based on the force method. Although the EIFM method formulated by Wang and Senatore [8] is equivalent and is more intuitive than SVD-FM, we have chosen to continue using the force method due to its familiarity and the convenience of extending our previous codes to this application. A structure comprising b beams, j joints, and c nodal constraints. The equilibrium (H) is expressed as follows.

$$\mathbf{H}t = P \tag{1}$$

Where t and P are the internal and external forces, including axial, bending, and twisting moments for a frame system, respectively, the

Table 1
Nodal coordinates of the egg-shaped numerical model (in mm).

Joints	X	Y	Z
1	0	1000	0
2–9	200.677, 141.9, 0, −141.9, 200.677, −141.9, 0, 141.9	925	0, 141.9, 200.677, 141.9, 0, −141.9, 200.677, −141.9
10–17	241.1262, 99.8778, −99.8778, −241.1262, −241.1262, −99.8778, 99.8778, 241.1262	840.6	99.8778, 241.1262, 241.1262, 99.8778, −99.8778, −241.1262, −241.1262, −99.8778
18 - 25	321.3093, 227.2, 0, −227.2, −321.3093, −227.2, 0, 227.2	756.2	0, 227.2, 321.3093, 227.2, 0, −227.2, −321.3093, −227.2
26 - 33	315.2083, 130.5636, −130.5636, −315.2083, −315.2083, −130.5636, 130.5636, 315.2083	669.3	130.5636, 315.2083, 315.2083, 130.5636, −130.5636, −315.2083, −315.2083, −130.5636
34 - 41	361.0487, 255.30, −255.3, −361.0487, −255.3, 0, 255.3	582.4	0, 255.3, 361.0487, 255.3, 0, −255.3, −361.0487, −255.3
42 - 49	328.6659, 136.1379, −136.1379, −328.6659, −328.6659, −136.1379, 136.1379, 328.6659	501.2	136.1379, 328.6659, 328.6659, 136.1379, −136.1379, −328.6659, −328.6659, −136.1379
50 - 57	350.4421, 247.8, 0, −247.8, −350.4421, −247.8, 0, 247.8	402	0, 247.8, 350.4421, 247.8, 0, −247.8, −350.4421, −247.8
58 - 65	299.9869, 124.2586, −124.2586, −299.9869, −299.9869, −124.2586, 124.2586, 299.9869	340.8	124.2586, 299.9869, 299.9869, 124.2586, −124.2586, −299.9869, −299.9869, −124.2586
66 - 73	298.9647, 211.4, 0, −211.4, −298.9647, −211.4, 0, 211.4	261.6	0, 211.4298.9647, 211.4, 0, −211.4, −298.9647, −211.4
74 - 81	226.36293.7622 −93.7622 −226.362 −226.362 −93.762293.7622226.362	182.4	93.7622, 226.362, 226.362, 93.7622, −93.7622, −226.362, −226.362, −93.7622
82 - 90	191.0603, 135.1, 0, −135.1, −191.0603, −135.1, 0, 135.1	103.2	0, 135.1, 191.0603, 135.1, 0, −135.1, −191.0603, −135.1
91	0	0	0

Table 2
Joint connectivity of the egg-shaped numerical model.

Members	Joint connectivity
1 –8	1 –2, 1 –3, 1 –4, 1 –5, 1 –6, 1 –7, 1 –8, 1 –9
9 –18	2 –10, 10 –19, 19 –27, 27 –36, 36 –44, 44 –53, 53 –61, 61 –70, 70 –78, 78 –87
19 –28	3 –11, 11 –20, 20 –28, 28 –37, 37 –45, 45 –54, 54 –62, 62 –71, 71 –79, 79 –88
29 –38	4 –12, 12 –21, 21 –29, 29 –38, 38 –46, 46 –55, 55 –63, 63 –72, 72 –80, 80 –89
39 –48	5 –13, 13 –22, 22 –30, 30 –39, 39 –47, 47 –56, 56 –64, 64 –73, 73 –81, 81 –82
49 –58	6 –14, 14 –23, 23 –31, 31 –40, 40 –48, 48 –57, 57 –65, 65 –66, 66 –74, 74 –83
59 –68	7 –15, 15 –24, 24 –32, 32 –41, 41 –49, 49 –50, 50 –58, 58 –67, 67 –75, 75 –84
69 –78	8 –16, 16 –25, 25 –33, 33 –34, 34 –42, 42 –51, 51 –59, 59 –68, 68 –76, 76 –85
79 –88	9 –17, 17 –18, 18 –26, 26 –35, 35 –43, 43 –52, 52 –60, 60 –69, 69 –77, 77 –86
89 –98	2 –17, 17 –25, 25 –32, 32 –40, 40 –47, 47 –55, 55 –62, 62 –70, 70 –77, 77 –85
99 –108	3 –10, 10 –18, 18 –33, 33 –41, 41 –48, 48 –56, 56 –63, 63 –71, 71 –78, 78 –86
109 –118	4 –11, 11 –19, 19 –26, 26 –34, 34 –49, 49 –57, 57 –64, 64 –72, 72 –79, 79 –87
119 –128	5 –12, 12 –20, 20 –27, 27 –35, 35 –42, 42 –50, 50 –65, 65 –73, 73 –80, 80 –88
129 –138	6 –13, 13 –21, 21 –28, 28 –36, 36 –43, 43 –51, 51 –58, 58 –66, 66 –81, 81 –89
139 –148	7 –14, 14 –22, 22 –29, 29 –37, 37 –44, 44 –52, 52 –59, 59 –67, 67 –74, 74 –82
149 –158	8 –15, 15 –23, 23 –30, 30 –38, 38 –45, 45 –53, 53 –60, 60 –68, 68 –75, 75 –83
159 –168	9 –16, 16 –24, 24 –31, 31 –39, 39 –46, 46 –54, 54 –61, 61 –69, 69 –76, 76 –84
169 –176	82 –90, 83 –90, 84 –90, 85 –90, 86 –90, 87 –90, 88 –90, 89 –90
Axial members	18 –19, 20 –21, 22 –23, 24,25, 66 –67, 68 –69,70 –71, 72 –73

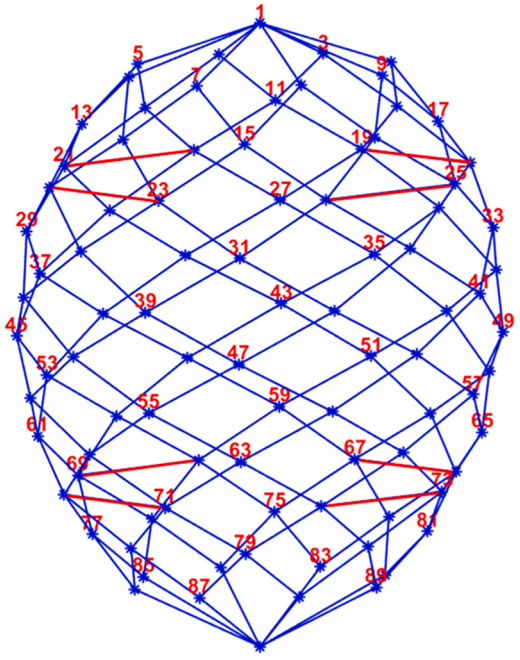

Fig. 2. The single-layer egg-shaped structure with eight additional bars and odd joint numbers.

compatibility matrix (C), which is the transpose of H, can be written as follows.

$$\mathbf{C}d = e \tag{2}$$

Where d and e are external and internal deformations, respectively, the flexibility matrix (F) relating internal forces and deformation is written as.

$$\mathbf{F}t = e \tag{3}$$

The relationships of the three matrices are illustrated in Fig. 1.

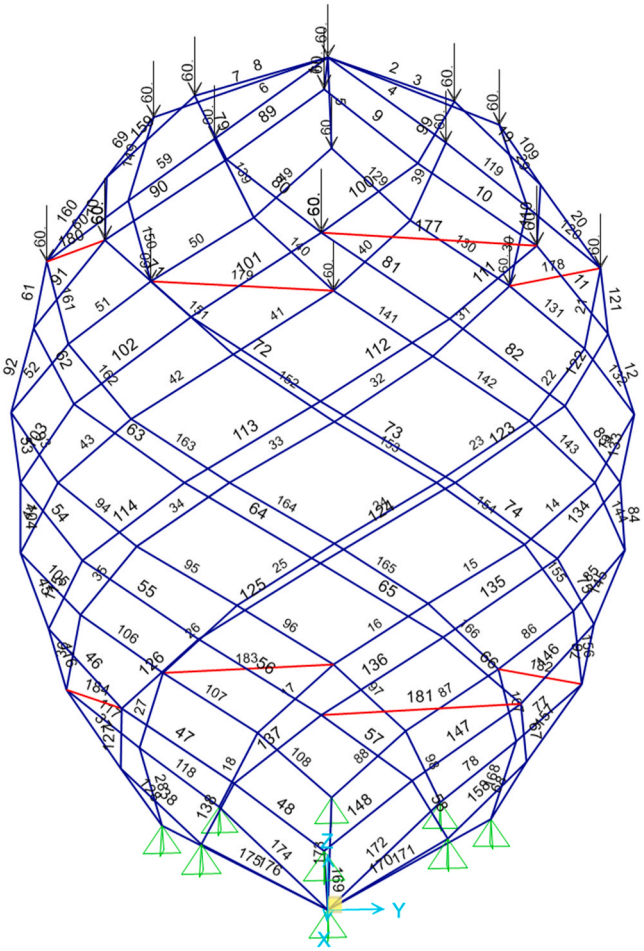

Fig. 3. Numerical model with eight additional bars, member numbering, support reactions, and loadings.

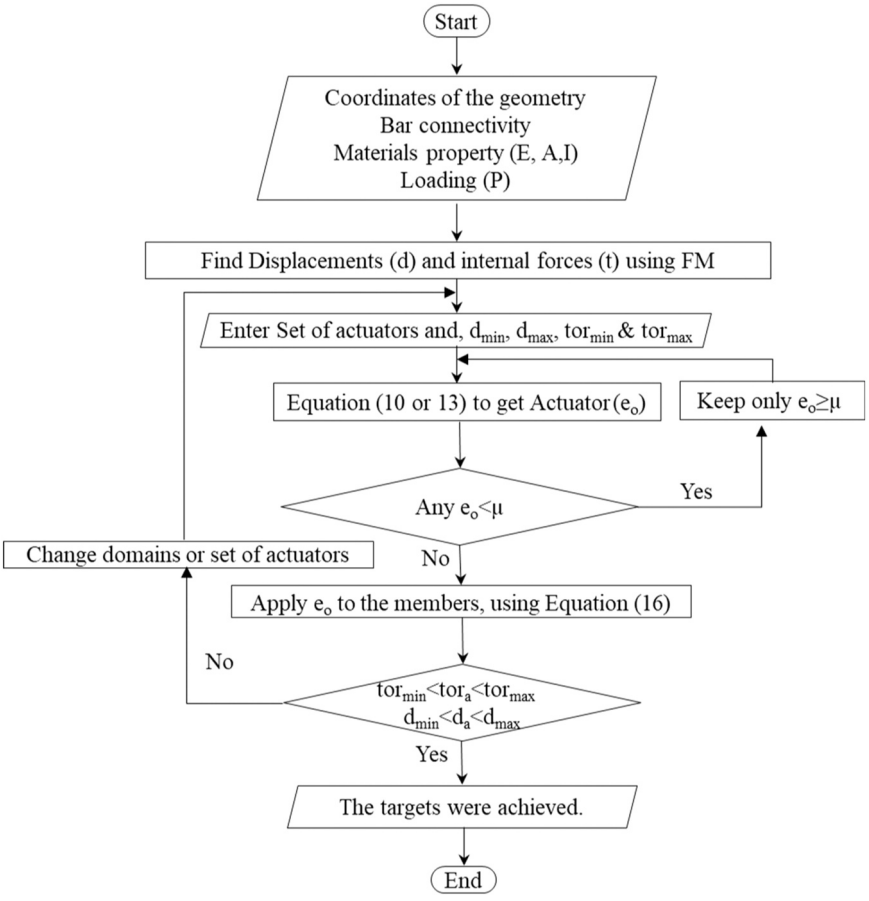

Fig. 4. Flow diagram of the algorithm applied in this work.

In some cases, such as structural imperfection or, in our case, altering bar length (e_o) to adjust shape and stress, the flexibility matrix is written as:

$$e = e_o + \mathbf{F}t \tag{4}$$

The internal force (t) can be expressed as follows:

$$t = t_H + \mathbf{S}\alpha \tag{5}$$

Where t is characterized by two components: t_H, which is in equilibrium with P but may not satisfy the compatibility, and the second part is independent states of self-stress (**S**). While α is the vector of (b-r), b is the number of bars of a structure, and r is the rank of the equilibrium matrix (**H**). Substituting (5) into (3) gives

$$e = e_o + \mathbf{F}(t_H + \mathbf{S}\alpha) \tag{6}$$

The compatibility of a set of e can be determined by checking if it belongs to the set of compatible column spaces of C. e must be orthogonal to the left-null space of **C**, which is also the null space of **H** since **H** and **C** are transposed of each other; thus, the condition of compatibility is $S^T e = 0$, or $\mathbf{S}^T e_o + \mathbf{S}^T\mathbf{F}(t_H + \mathbf{S}\alpha) = 0$ thus.

$$-\alpha = \left(\mathbf{S}^T\mathbf{F}\mathbf{S}\right)^{-1}\left[\mathbf{S}^T e_o + \mathbf{S}^T\mathbf{F}t_H\right] \tag{7}$$

In the force method, the process of obtaining internal forces and external displacements involves substituting α in (5) and the compatibility equation. The relation of bar length change and nodal coordinates is presented in Eqs. (8 and 9) by substituting (7) in (6) and then in the compatibility equation.

$$\begin{aligned} \mathbf{C}d &= e_o + \mathbf{F}\left(t_H - \mathbf{S}\left(\mathbf{S}^T\mathbf{F}\mathbf{S}\right)^{-1}\left[\mathbf{S}^T e_o + \mathbf{S}^T\mathbf{F}t_H\right]\right) \\ d &= \mathbf{C}^+ e_o + \mathbf{C}^+\mathbf{F}\left(t_H - \mathbf{S}\left(\mathbf{S}^T\mathbf{F}\mathbf{S}\right)^{-1}\left[\mathbf{S}^T e_o + \mathbf{S}^T\mathbf{F}t_H\right]\right) \\ d &= \left[\mathbf{C}^+ - \mathbf{C}^+\mathbf{F}\mathbf{S}\left(\left(\mathbf{S}^T\mathbf{F}\mathbf{S}\right)^{-1}\mathbf{S}^T\right)\right]e_o + \left[\mathbf{C}^+\mathbf{F} - \mathbf{C}^+\mathbf{F}\mathbf{S}\left(\mathbf{S}^T\mathbf{F}\mathbf{S}\right)^{-1}\mathbf{S}^T\mathbf{F}\right]t_H \end{aligned} \tag{8}$$

$$\mathbf{Y}e_o + d_p = d_t \tag{9}$$

Y is $\mathbf{C}^+ - \mathbf{C}^+\mathbf{F}\mathbf{S}(\mathbf{S}^T\mathbf{F}\mathbf{S})^{-1}\mathbf{S}^T$ that relates external deformation and structural members length change, while d_p is $[\mathbf{C}^+\mathbf{F} - \mathbf{C}^+\mathbf{F}\mathbf{S}(\mathbf{S}^T\mathbf{F}\mathbf{S})^{-1}\mathbf{S}^T\mathbf{F}]t_H$ which is also equal to $\mathbf{C}^+e$, while $\mathbf{C}^+$ is the pseudo inverse of **C** and d_t is the targeted external displacements. Eq. (9) is now expressed to let the displacements have a value within a given domain [d_{min} d_{max}] as follows [32].

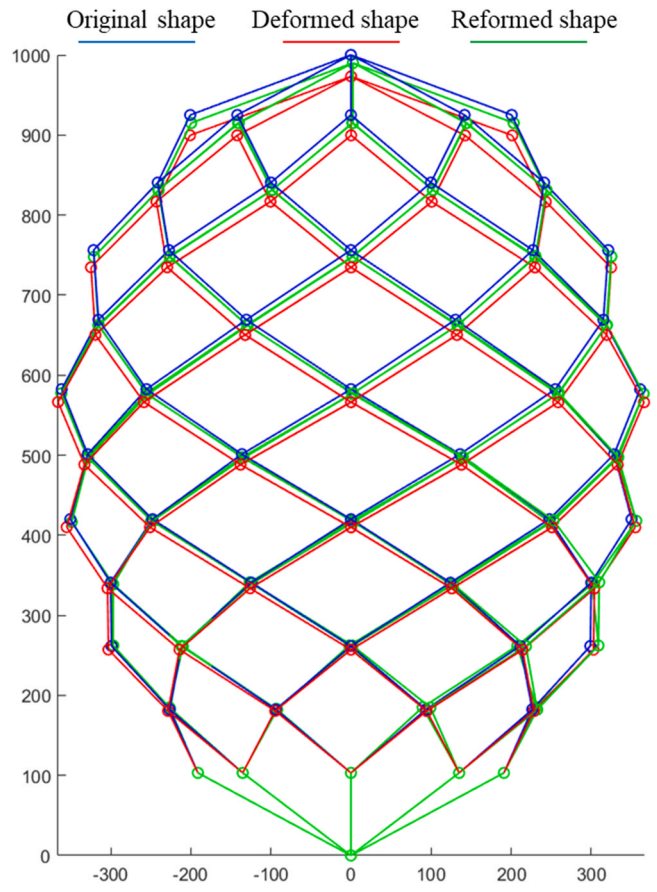

Fig. 5. Space frame configuration before loading, deformed (after loading), and reformed shapes.

$$d_{\min} \le \mathbf{Y}e_o + d_p \le d_{\max} \tag{10}$$

The original size of the Y matrix is (6j-c, 6b); we are only interested in the joint translations. Thus, the matrix size is reduced to (3j-c, b), and all internal deformation parameters except bar length change (e_o) will be removed. The algorithm iteratively removes inactive beams, retaining only the active beams whose required length changes exceed 0.1 mm, as detailed in Section ↱2.3.

$$\theta_{y1}\theta_{z1}\mathrm{e}_o\beta\theta_{y2}\theta_{z2}$$

$$Y = \begin{bmatrix} c_{11} & c_{12} & c_{13} & c_{14} & c_{15} & c_{16} \\ c_{21} & c_{22} & c_{23} & c_{24} & c_{25} & c_{26} \\ c_{31} & c_{32} & c_{33} & c_{34} & c_{35} & c_{36} \\ & & & c_{44} & & \\ & & & & c_{55} & \\ & & & & & c_{66} \end{bmatrix} \begin{matrix} \mathrm{d}_{x1} \\ \mathrm{d}_{y1} \\ \mathrm{d}_{z1} \\ \Psi_{y1} \\ \Psi_{z1} \\ \eta \end{matrix}$$

where θ and Ψ are external and internal rotations, d is the nodal displacement e_o is the bar length alteration, β and η are the external and internal angles of the twist. In this study, the relation of torsion and e_o is derived by subbing (10) in (8) as follows.

$$\begin{aligned} t &= t_H - \mathbf{S}\left(\mathbf{S}^T\mathbf{F}\mathbf{S}\right)^{-1}\left[\mathbf{S}^T e_o + \mathbf{S}^T\mathbf{F}t_H\right]\Big) \\ &= \left[I - \mathbf{S}\left(\mathbf{S}^T\mathbf{F}\mathbf{S}\right)^{-1}\mathbf{S}^T\mathbf{F}\right]t_H - \left[\mathbf{S}\left(\mathbf{S}^T\mathbf{F}\mathbf{S}\right)^{-1}\mathbf{S}^T\right]e_o \end{aligned} \tag{11}$$

$$tor_t = tor_p - \mathbf{Z}e_o \tag{12}$$

Where tor_{t} is the targeted torsion value, tor_{p} is the torsion due to loading, and **Z** is the matrix relates twisting moment and e_o. The size of the original **Z** matrix is (6*b*, 6*b*).

This study deals with the effect of bar length change (3rd column of Z) on the torsion (4th row of Z). After implementing the optimization algorithm, the Z matrix is reduced to (b, b), and the column size will be reduced, i.e., only active beams will remain.

$$\theta_{y1}\theta_{z1}\mathrm{e}_o\beta\theta_{y2}\theta_{z2}$$

$$Z = \begin{bmatrix} c_{11} & & c_{13} & & & & \\ & c_{22} & c_{23} & & & & \\ & & c_{33} & & & & \\ c_{41} & c_{42} & c_{43} & c_{44} & c_{45} & c_{46} & \\ & & c_{53} & & c_{55} & & \\ & & c_{63} & & & c_{66} & \end{bmatrix} \begin{matrix} \mathrm{m}_{y1} \\ \mathrm{m}_{z1} \\ \mathrm{t}_n \\ \mathrm{tor} \\ \mathrm{m}_{y2} \\ \mathrm{m}_{z2} \end{matrix}$$

m is the bending moment, t_{n} is the axial force, and *tor* is the twisting moment. In reality, requiring control over one (displacement or torsion) will also have some effects on the other. For example, while it is critical to restore the structure's shape to a prescribed profile via member length change, it is also necessary that the resultant set of $\mathrm{e_o}$ does not increase torsion to dangerous levels. In many situations, there is thus a need to be able to simultaneously control both the shape geometry and the element torsional forces via the same set of $\mathrm{e_o}$. Thus, the combined equations become

$$\begin{aligned} d_{\min} &\le \mathbf{Y}e_o + d_p \le d_{\max} \\ tor_{\min} &\le \mathbf{Z}e_o - tor_p \le tor_{\max} \end{aligned} \tag{13}$$

Where, $\mathrm{tor_p}$ is the induced twisting moments in members due to loadings or reducing shape deformation and $[tor_{\min}\ tor_{\max}]$ is the desired domain of the twisting moment after applying the length changing of active bars. Moreover, **Z** is the matrices that link the twisting moment in members with the structural elements equipped with actuators. e_o is the required change of length of the actuators to keep the torsion in all structure members within the allowable domain. The optimization function, presented in Eq. (14), is subjected to Eqs. (10, 12, and 13) to minimize the actuator length changes. In addition, removing actuators that are required to perform length changes smaller than 0.1 mm (μ) in this study can reduce the total number of actuators.

$$\min f(x) = \sum_{i=1}^{n} e_{oi} \tag{14}$$

Our numerical model employs the linprog function, which uses the interior point optimization algorithm. We also use fmincon, which uses interior point or SQP. These algorithms iteratively search for a set of e_o

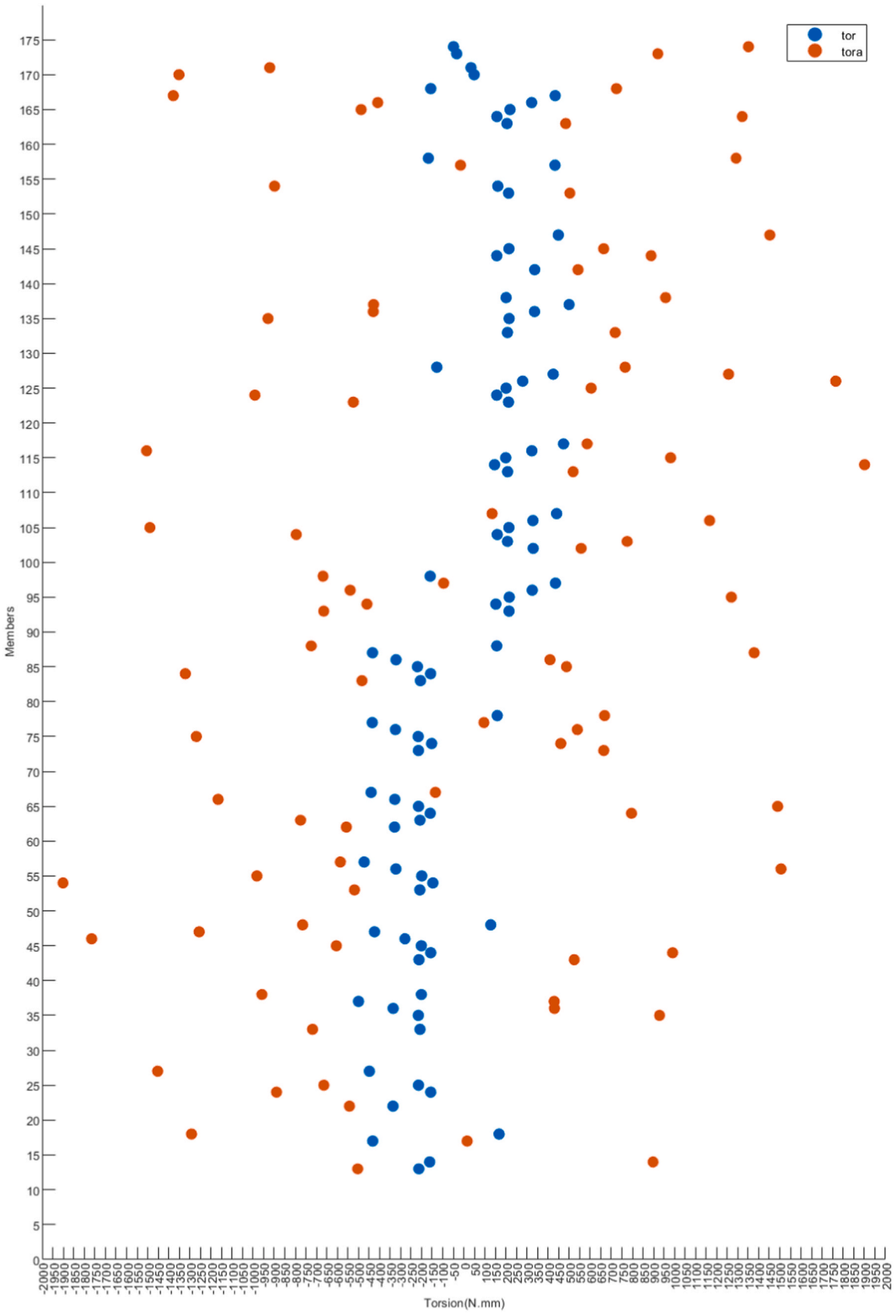

Fig. 6. The twisting moment in members that are greater than 400 N.mm before /after shape adjustment.

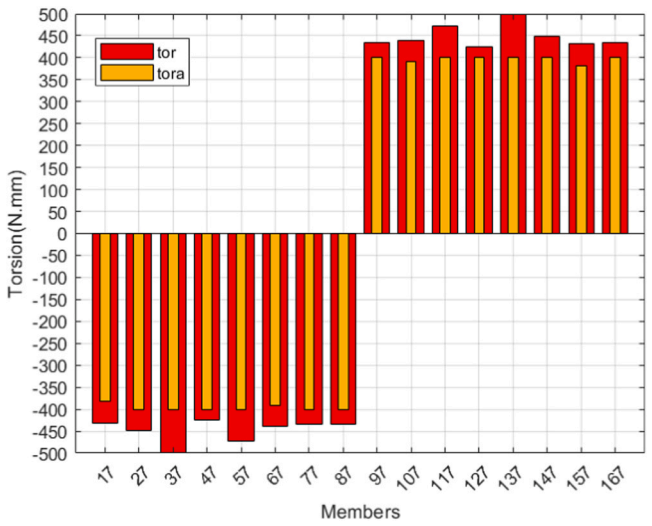

Fig. 7. Twisting moment in critical members before/after actuator length changes using Eq. 12.

that provide a minimum summation of actuator length changes while considering the constraints, and the upper bound (U_b) and lower bound (L_b) for actuator length change.

$$|L_b| \leq |e_o| \leq |U_b| \tag{15}$$

(L_b and U_b) have been thoughtfully determined in this paper, considering the members' length and the actuator's length change capacity to guarantee the practicality and real-world applicability of the model. The limits of −5 mm and 5 mm have been set to avoid any significant changes in the structural geometry. In practice, reducing the number of actuators is more cost-effective than making inefficient or less effective actuator length changes; thus, the actuators required to perform length changes smaller than 0.1 mm (μ) will be removed iteratively. After applying the obtained e_o, the twisting moment in members (tor_a) and nodal displacement (d_a) are obtained as follows.

$$\begin{aligned} tor_a &= tor_p - \mathbf{Z} * e_o \\ d_a &= d_p + \mathbf{Y} * e_o \end{aligned} \tag{16}$$

2.2. The numerical model

A single-layer egg-shaped space frame is numerically modeled and analyzed in MATLAB. The structure's thin skin is highly susceptible to distortion, making precision crucial and imperfections unacceptable. Similar structures have already been studied for shape control [12], where twisting moments were not considered but were found to be very high after reducing deformation. The numerical model is formed by 90 joints connected by 176 flexural members. Eight additional axial members were horizontally added to mitigate the deformed shape. The members are made of 6 mm diameter steel with Young's modulus of 200 GPa. Tables 1 and 2 give the coordinate system of the nodes and the members' connectivity. Figs. 2 and 3 show the structures' nodal and member numbering and visualize the supported nodes and loadings. The numerical model is supported at the nine bottom nodes (Joints 82 - 90) in the x, y, and z directions. Nodes 1–9 and 18–25 were subjected to 60 N downward loading (see Fig. 3), which induced a noticeable deformation, as studied by Saeed *et al.* [12], to reduce the nodal displacement.

2.3. Computational procedure

After inputting the structural geometry and loadings, nodal displacement and torsion in all members are determined using SVD-FM. In this stage, limits for the nodal displacements and torsional members are assumed, and the minimum actuator length change is determined through Eqs. (10, 12, and 13) in several iterations, as presented in Fig. 4. Twisting moments in members and nodal displacements and the amount of length change per actuator are considered. First, it is assumed that all structural members are equipped with actuators; then, step by step, the actuators that are required to perform a length change smaller than 0.1 mm ($e_o < 0.1$ mm) are removed. It should be noted that the proposed approach operates through an iterative process guided by a heuristic that takes into account a minimum threshold for the necessary change in actuator length. However, this method does not ensure any optimal conditions regarding the number of actuators needed or their positions.

3. Numerical example

3.1. Case 1 deformation control by member length change

In this case, the deformed shape of a single-layer space frame has been reshaped after loading. The maximum displacement occurs at the top joint (J1) in the direction of loading. The goal is to keep the nodal displacements within ± 10 mm in all directions using Eq. 10. Fig. 5 shows the structural configuration in three stages. However, the shape is controlled through actuating Member [3 4 5 8 28 38 58 68 78 98 108 118 138 148] by [1.1498 1.9896 1.1498 0.4998 0.3715 6.6073 4.9097 5.6454 0.2077 0.2077 5.6454 4.9097 6.6073 0.3715] mm respectively within ± 10 mm for all nodes. Despite mitigating the deformation by actuating some bars, it caused a significant increase in twisting moments of some members. Fig. 6 shows the momentous change in twisting moment in critical members from 500 N.mm to just under 2000 N.mm.

If only Eq. 12 is implemented to control twisting moment without regard to the shape, the twisting moment can be controlled within [−400 400] N.mm in all members through actuating Members [27 47 57 67 77 87 97 107 117 127 147 167] with [−0.13373 −0.17404 −0.14832 −0.13572 −0.057838 −0.10709 -−0.057838 −0.13572 −0.14832 −0.17404 −0.13373 −0.10709] mm respectively. However, the twisting moment is controlled, as presented in Fig. 7. The maximum nodal displacement is −13.5 mm, which is slightly higher than the maximum displacement before mitigating the twisting moment.

Due to the substantial increase in the twisting moment after shape adjustment and noticeable displacement in controlling only the twisting moment, both aspects simultaneously should be considered. Now, Eq. 13 is implemented to reduce the deformed shape and control the twisting moment within ± 400 N.mm in all members simultaneously. It can be seen from Fig. 8 that the twisting moment in all members kept within ± 400 N.mm. Meanwhile, the nodal displacement in all nodes stayed

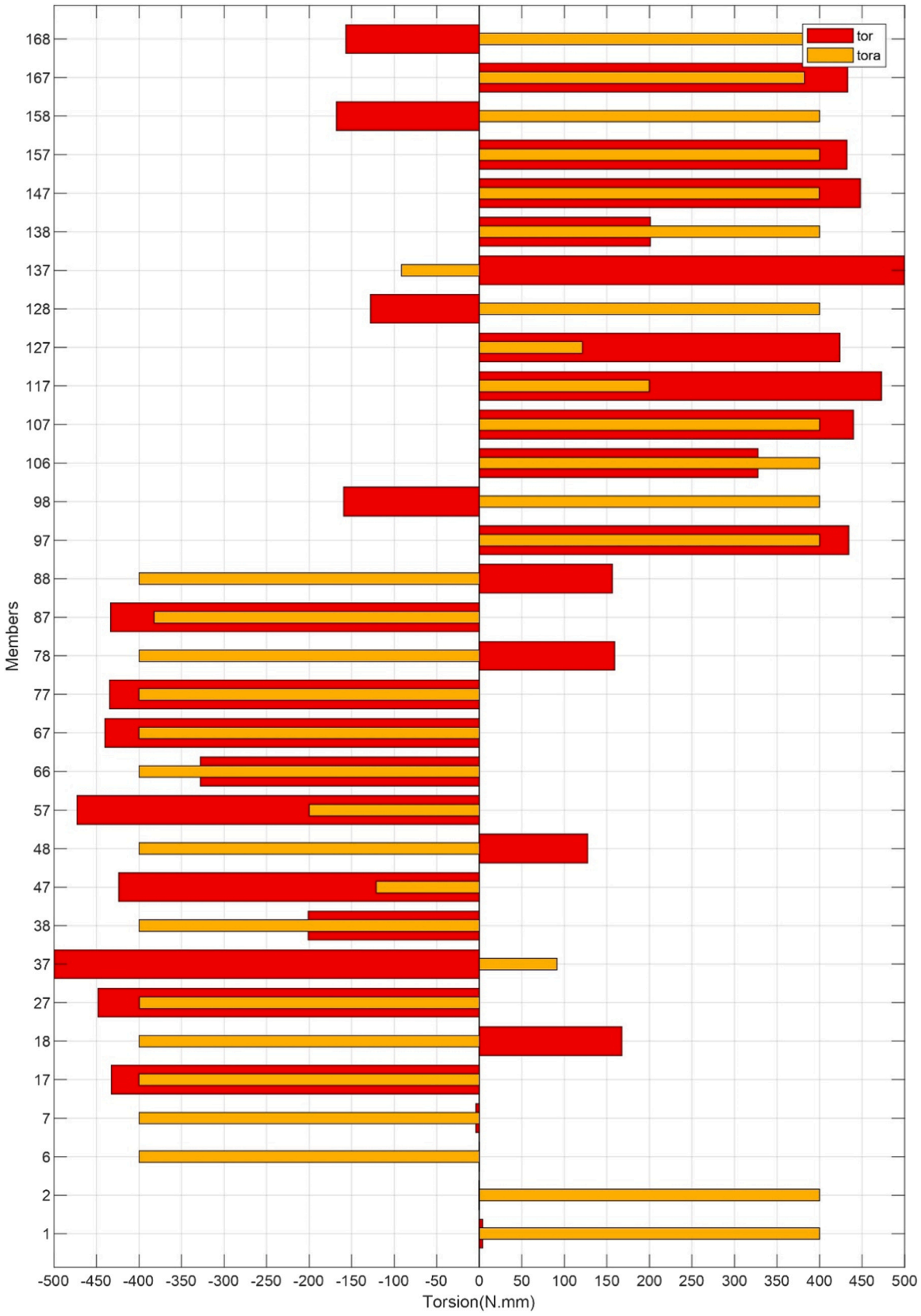

Fig. 8. Twisting moment in critical members before/after reshaping using Eq. 10.

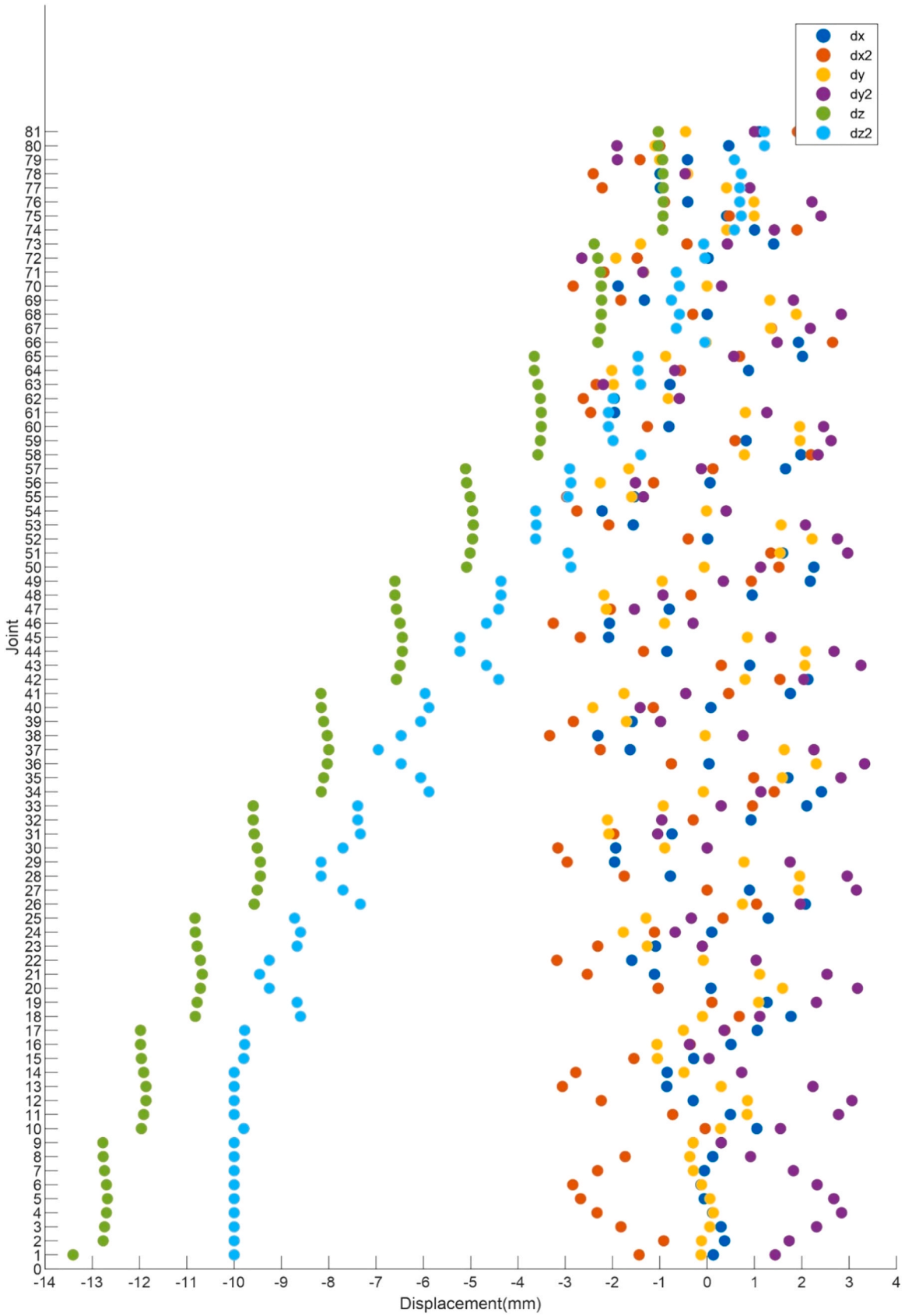

Fig. 9. Nodal displacements before /after actuator length changes of the space frame using Eq. 10.

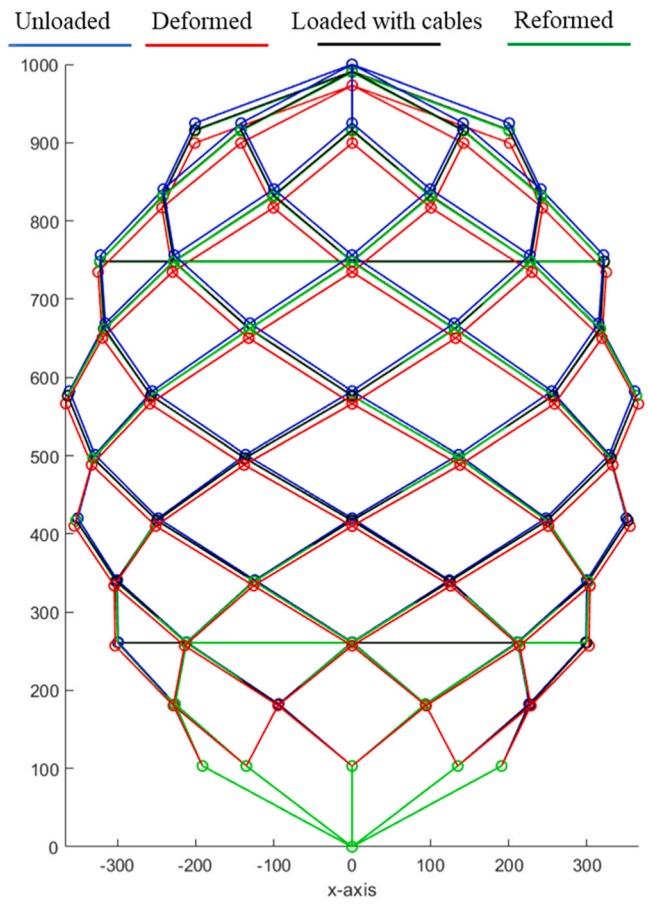

Fig. 10. Structural configuration in four various stages.

within ± 10, as presented in Fig. 9. Fig. 8 shows a rapid increase in twisting moment in Members 1, 2, 6, and 7 and changes from negative twisting moment to positive in Members 37, 96, 128, 158, and 168 and from positive to negative in Members 18, 48, 78, 88, 137.

3.2. Deformation mitigation by adding extra members

Saeed *et al.* [12] investigated several scenarios for adding extra horizontal members to reduce the deformation of the single-layer egg-shaped space frame. They found that a suitable case is adding eight extra bars in the upper and lower quarters of the structure's height (See Fig. 3) to prevent stress concentration in specific areas and effectively reduce deformation across the structure. This is evidenced by the mitigation of the maximum displacement in the top node from −13.41 mm to −8.7 mm (See Fig. 10). However, this addition did cause an increase in twisting moments in some members, from 499.6 N.mm to up to 576 N.mm. Nonetheless, using Eq. 13 allowed us to maintain control over the twisting moment within the limit [−400 400] N.mm, as shown in Fig. 11 and keep the nodal displacements in all nodes within [−10 10] mm.

3.3. Computational optimization

Two distinct functions were utilized in MATLAB: linprog for linear optimization problems and fmincon for both linear and nonlinear problems. In Case 1, which involves displacement control without considering the twisting moment, the number of iterations and computational time were analyzed to compare the performance of these two functions. Table 3 indicates that both functions successfully determined the optimal actuator length change of 40.27 mm. The fmincon function achieved this optimal solution in twenty-eight iterations and 0.15 s using the interior point algorithm and in fifteen iterations and 0.03 s using the SQP algorithm. Conversely, the linprog function, employing the interior point algorithm, attained the optimal solution in only ten iterations and 0.05 s. Both the interior point and SQP methods in fmincon converged close to the optimal solution by the 23rd and 10th iterations, respectively, as evidenced by the first-order optimality (FOO) conditions. Similarly, the interior point method in linprog approached the optimal solution by the 8th iteration, with the complementary slackness conditions (CSC) approaching zero.

4. Conclusion

A simple technique has been presented in this work to simultaneously control the deformed shape and twisting moments in members of space frames through axial length changing of members. The technique used and developed in this work can reduce twisting moments within prescribed limits. The approach is based on the force method coupled with optimization algorithms to minimize the actuator length changes and keep twisting moments within the limit [−400 400] N.mm. It also keeps the nodal displacements within [−10 10] mm. In addition, the targets are obtained by minimizing actuator length changes by using optimization algorithms through the linprog and Fmincon functions in MATLAB. The numerical model was modeled using MATLAB and SAP2000 software to verify the accuracy of the technique.

CRediT authorship contribution statement

Najmadeen Saeed: Writing – review & editing, Software, Methodology, Conceptualization. **Ahmed Manguri:** Writing – review & editing, Writing – original draft, Visualization, Validation, Software, Methodology, Formal analysis, Conceptualization. **Robert Jankowski:** Writing – review & editing, Supervision, Conceptualization.

Declaration of Competing Interest

The authors declare that they have no known competing financial interests or personal relationships that could have appeared to influence the work reported in this paper.

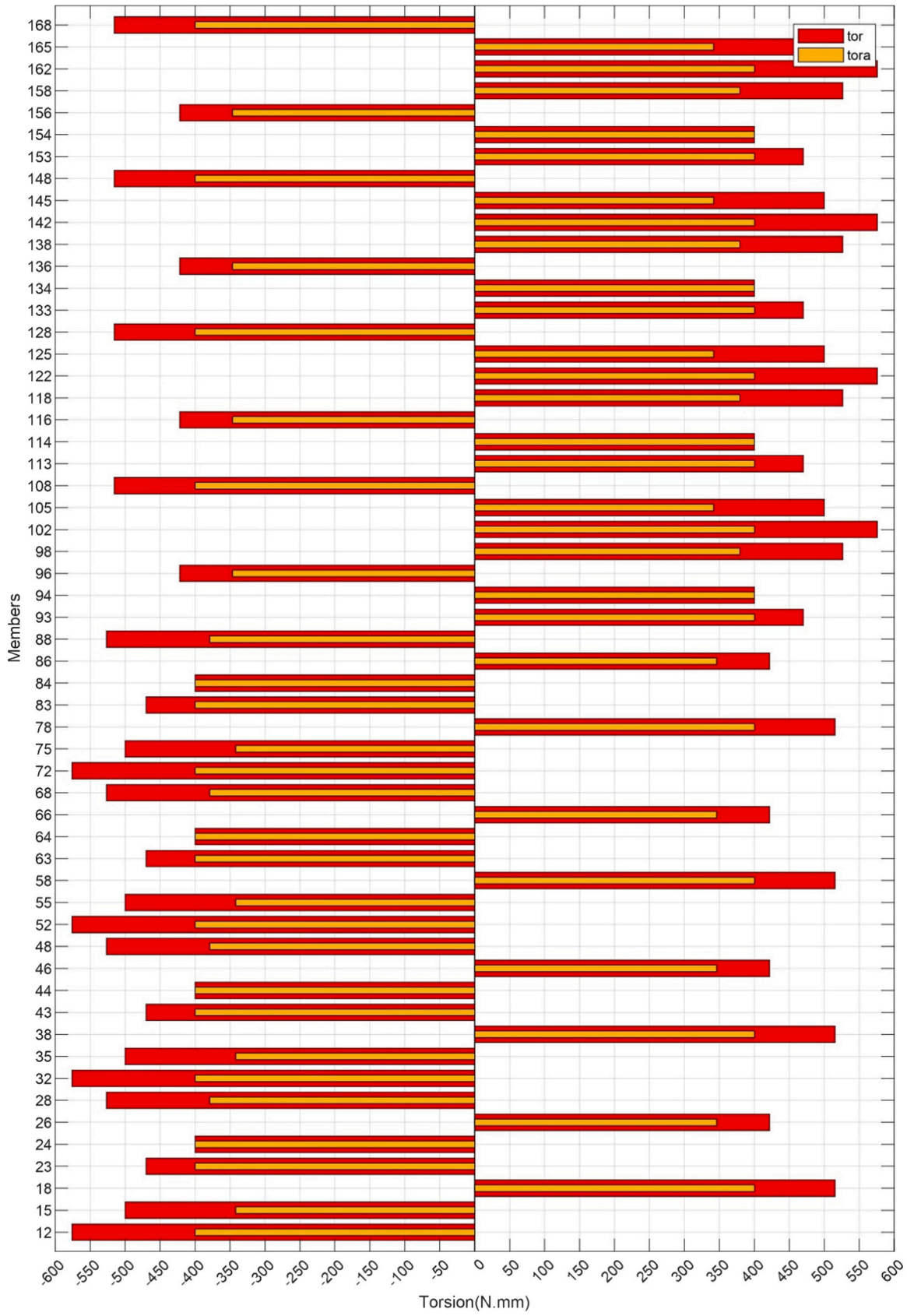

Fig. 11. Twisting moment in critical members before /after actuator length changes using Eq. 13.

Table 3
Total actuator length change using two functions.

Function	fmincon				linprog	
Algorithm	Interior point		SQP		Interior point	
Iterations	e_o (mm)	FOO	e_o (mm)	FOO	e_o (mm)	SCS
0	14.00	2	14.00	1.00	231.51	106.1745
1	16.41	1.769	41.41	2.87	202.33	38.2321
2	38.43	0.3843	40.91	0.43	107.65	13.6801
3	41.83	0.3744	40.54	0.12	63.35	4.5501
4	41.36	0.1846	40.52	0.02	58.45	1.5522
5	41.65	0.1001	40.52	0.02	45.30	0.4109
6	40.68	0.0548	40.51	0.02	40.74	0.0719
7	40.70	0.0312	40.47	0.02	40.46	0.0264
8	40.72	0.02	40.29	0.02	40.27	0.0006
9	40.56	0.0185	40.29	0.00	40.27	0
10	40.54	0.0185	40.29	0.00	40.27	0
11	40.43	0.0185	40.29	0.00	-	-
12	40.33	0.017	40.29	0.00	-	-
13	40.36	0.0121	40.27	0.00	-	-
14	40.34	0.0042	40.27	0.00	-	-
15	40.30	0.0023	40.27	0.00	-	-
16	40.31	0.0023	-	-	-	-
17	40.31	0.0023	-	-	-	-
18	40.30	0.0023	-	-	-	-
19	40.29	0.0023	-	-	-	-
20	40.28	0.0015	-	-	-	-
21	40.29	0.0015	-	-	-	-
22	40.28	0.0009	-	-	-	-
23	40.27	0.0002	-	-	-	-
24	40.27	0	-	-	-	-
25	40.27	0	-	-	-	-
26	40.27	0	-	-	-	-
27	40.27	0	-	-	-	-
28	40.27	0	-	-	-	-
Time (sec)	0.15		0.03		0.05	

References

[1] Yamaguchi H. Spatial structure of the front garden and site arrangement in the Honbou and Tacchu of Daitokuji and Myoshinji temples: study on spaces that connect the interior and exterior. Jpn Archit Rev 2022;5(4):445–57. https://doi.org/10.1002/2475-8876.12274.

[2] Chatti S. Production of profiles for lightweight structures. BoD–Books on Demand; 2006.

[3] E. Sysoeva Preconditions of emergence of large-span buildings in the world in *MATEC Web of Conferences* 2016 EDP Sciences, doi: 10.1051/matecconf/20168602004.

[4] Weeks CJ. Static shape determination and control of large space structures: I. The flexible beam. J Dyn Syst, Meas, Control 1984;106(4):261–6. https://doi.org/10.1115/1.3140683.

[5] Haftka RT, Adelman HM. An analytical investigation of shape control of large space structures by applied temperatures. AIAA J 1985;23(3):450–7. https://doi.org/10.2514/3.8934.

[6] Kwan A, Pellegrino S. Prestressing a space structure. AIAA J 1993;31(10):1961–3. https://doi.org/10.2514/3.11876.

[7] Reksowardojo AP, Senatore G. A proof of equivalence of two force methods for active structural control. Mech Res Commun 2020;103:103465. https://doi.org/10.1016/j.mechrescom.2019.103465.

[8] Wang Y, Senatore G. Extended integrated force method for the analysis of prestress-stable statically and kinematically indeterminate structures. Int J Solids Struct 2020;202:798–815. https://doi.org/10.1016/j.ijsolstr.2020.05.029.

[9] Saeed NM, Kwan ASK. Simultaneous displacement and internal force prescription in shape control of pin-jointed assemblies. AIAA J 2016;54(8):2499–506. https://doi.org/10.2514/1.J054811.

[10] Saeed NM, Manguri AAH, Adabar AM. Shape and force control of cable structures with minimal actuators and actuation. Int J Space Struct 2021;36(3):241–8. https://doi.org/10.1177/09560599211045851.

[11] Zhang H, Lu J, Gong P, Li N. Member control efficiency and shape control capability of a loaded cable dome. Structures 2023;58:105378. https://doi.org/10.1016/j.istruc.2023.105378.

[12] N. Saeed A. Manguri S. Abdulkarim A. Shekha Shape Restoration of Deformed Egg-Shaped Single Layer Space Frames 2019 International Conference on Advanced Science and Engineering (ICOASE) 2019 IEEE, Duhok, Kurdistan Region, Iraq doi: 10.1109/ICOASE.2019.8723714.

[13] Reksowardojo Arka, P, Senatore G, Bischoff M, Blandini L. Design and control benchmark of rib-stiffened concrete slabs equipped with an adaptive tensioning system. J Struct Eng 2024;150(1):04023200. https://doi.org/10.1061/JSENDH.STENG-12320.

[14] Reksowardojo AP, Senatore G, Bischoff M, Blandini L. Design and control of high-speed railway bridges equipped with an under-deck adaptive tensioning system. J Sound Vib 2024;579:118362. https://doi.org/10.1016/j.jsv.2024.118362.

[15] Manguri A, Saeed N, Kazemi F, Szczepanski M, Jankowski R. Optimum number of actuators to minimize the cross-sectional area of prestressable cable and truss structures. Structures 2023;47:2501–14. https://doi.org/10.1016/j.istruc.2022.12.031.

[16] Senatore G, Wang Y. Topology optimization of adaptive structures: new limits of material economy. Comput Methods Appl Mech Eng 2024;422:116710. https://doi.org/10.1016/j.cma.2023.116710.

[17] Lan TT. Space frame structures. Struct Eng Handb 1999;13(4)).

[18] Ramaswamy G, Eekhout M, Suresh G. Analysis, design and construction of steel space frames. Thomas Telford,; 2002.

[19] Galishnikova V, Gebre T, Tupikova E, Niazmand M. The design guide for space frames with or without warping restraint at nodes. in *AIP Conference Proceedings*. AIP Publishing,; 2022. https://doi.org/10.1063/5.0099013.

[20] Bauchau OA, Craig JI. Torsion. In: Bauchau OA, Craig JI, editors. Structural Analysis. Dordrecht: Springer Netherlands; 2009. p. 261–95.

[21] Kollbrunner CF, Basler K. Torsion in structures: an engineering approach. Springer Science & Business Media,; 2013.

[22] Manguri A, Saeed N, Szczepanski M, Jankowski R. Bending Moment Control and Weight Optimization in Space Structures by Adding Extra Members in the Optimal Locations. Adv Sci Technol Res J 2023;17(4):313–24. https://doi.org/10.12913/22998624/169573.

[23] Rohilla S, Sebastian R. Resonant column and cyclic torsional shear tests on Sutlej river sand subjected to the seismicity of Himalayan and Shivalik hill ranges: a case study. Soil Dyn Earthq Eng 2023;166:107766. https://doi.org/10.1016/j.soildyn.2023.107766.

[24] Fu J, Chen S. Torsion in symmetric buildings due to soil-structure interaction: a discussion on code values of accidental eccentricity factor in seismic design. Earthq Eng Struct Dyn 2022;51(15):3461–78. https://doi.org/10.1002/eqe.3731.

[25] Anagnostopoulos S, Kyrkos M, Stathopoulos K. Earthquake induced torsion in buildings: critical review and state of the art. Earthq Struct 2015;8(2):305–77. https://doi.org/10.12989/eas.2015.8.2.305.

[26] Olivares CI, de la Llera JC, Poulos A. Torsion control in structures isolated with the triple friction pendulum system. Eng Struct 2020;216:110503. https://doi.org/10.1016/j.engstruct.2020.110503.

[27] Shook DA, Roschke PN, Lin P-Y, Loh C-H. Semi-active control of a torsionally-responsive structure. Eng Struct 2009;31(1):57–68. https://doi.org/10.1016/j.engstruct.2008.06.016.

[28] Xu YL, Shum KM. Multiple-tuned liquid column dampers for torsional vibration control of structures: theoretical investigation. Earthq Eng Struct Dyn 2003;32(2):309–28. https://doi.org/10.1002/eqe.227.

[29] Shum KM, Xu YL. Multiple-tuned liquid column dampers for torsional vibration control of structures: experimental investigation. Earthq Eng Struct Dyn 2002;31(4):977–91. https://doi.org/10.1002/eqe.133.

[30] Tena-Colunga A, Escamilla-Cruz JL. Torsional amplifications in asymmetric base-isolated structures. Eng Struct 2007;29(2):237–47. https://doi.org/10.1016/j.engstruct.2006.03.036.

[31] Tso Wai K. K., Static eccentricity concept for torsional moment estimations. J Struct Eng 1990;116(5):1199–212. https://doi.org/10.1061/(ASCE)0733-9445(1990)116:5(1199).

[32] Saeed NM, Manguri AA, Szczepanski M, Jankowski R, Haydar BA. Static shape and stress control of trusses with optimum time, actuators and actuation. Int J Civ Eng 2023;21(3):379–90. https://doi.org/10.1007/s40999-022-00784-3.